Meccanica (2006) 41:143–156
DOI 10.1007/s11012-005-1058-9

Tyre Wear Model: Validation and Sensitivity Analysis

FRANCESCO BRAGHIN*, FEDERICO CHELI, STEFANO MELZI and FERRUCCIO RESTA
Politecnico di Milano, Mechanical Engineering Department, Via La Masa 34-20156, Milan, Italy

(Received: 29 January 2005; accepted in revised form: 13 June 2005)

Abstract. Due to their many economic and ecological implications the possibility to predict tyre wear is of major importance to tyre manufacturers, fleet owners and governments. Based on these observations, in 2000 a three-year project named Tyre and Road Wear and Slip assessment (*TROWS*) was started. One of the *TROWS* objectives was to provide a tool able to numerically predict tyre global wear as well as to qualitatively determine the wear distribution. The proposed methodology combines a mathematical model of the tyre with an experimentally determined local friction and wear law. Thus, tyre abrasion due to each single manoeuvre can be determined.

Full-scale experimental tests were carried out with two Peugeot 406 cars on a public road course in Italy. Each car was equipped with a different set of tyres: one car was equipped with four all-season tyres (from now on called A tyres) and the other car was equipped with four winter tyres (from now on called B tyres). Both sets of tyres had a 195/65 R15 size. The collected data was used to validate the model. The methodology proved to give qualitatively good tyre wear predictions.

Key words: Tyre model, wear prediction, experimental comparison, sensitivity analysis.

1. Introduction

The aim of this work is to provide a simulation tool that takes into account both tyre structure and tyre tread design thus allowing to predict tyre wear for a given manoeuvre as function of road and vehicle characteristics. The same simulation tool could be used to determine those tyre structural and contact parameters that mostly affect tyre wear thus providing guidelines for tyre manufacturers on how to produce tyres with less environmental impact.

2. The Tyre Model

The proposed tyre model (from now on called *PaRRT* model, Physical Rigid Ring Tyre model) allows the simulation of any given manoeuvre starting from the time histories of the applied generalized hub forces, i.e., the longitudinal, lateral and vertical hub forces, the applied driving/braking torque and the imposed slip and camber angles. These input quantities may come from experimental measurements or from vehicle's multi-body simulations.

*Author of correspondence: E-mail: francesco.braghin@polimi.it

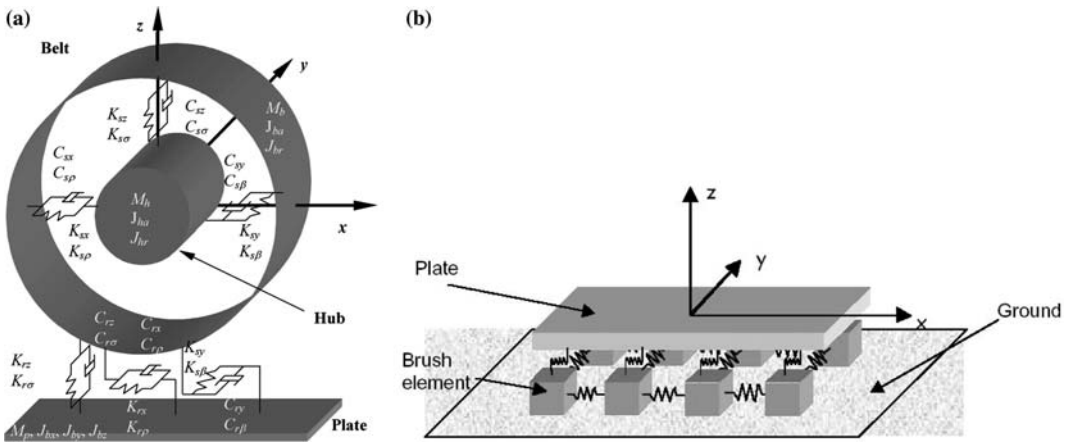

Figure 1. The tyre structural model (a) and the tyre contact model (b).

The model (described in detail in Ref. [1]) can be split into two interconnected substructures (Figure 1a and b): the tyre structural model and the tyre contact model (a 2D brush model).

2.1. The Tyre Structural Model

The tyre structural model (Figure 1a) is made up of three rigid bodies (a disc, a ring and a plate) that represent the hub, the belts and the contact area between tyre and road [1]. The tyre contact model is connected to the contact plate.

An absolute right hand reference system with z-axis taken upwards in vertical direction is adopted. With respect to this reference system, the motion of the three bodies representing the tyre structure is described: the hub and belts have six degrees of freedom each while the plate has only three degrees of freedom since its motion is bounded to be parallel to the ground.

The three rigid bodies that constitute the tyre structural model are linked to each other by means of elastic and viscous linear elements. Structural elements (parameters), connecting the disc and the ring, represent the behaviour of the sidewalls of the inflated tyre, while those connecting the ring and the plate, represent the effects of the local deformation of the belts near the contact area when a vertical load is applied. Tyre structural parameters may be identified in the frequency domain from FEA simulations carried out with a refined FE tyre model or in the frequency/time domain from experimental indoor tests [2]. It should be observed that these parameters are a function of the inflation pressure and of the applied vertical load at the hub but not of the tyre rolling speed. The validity of the *PaRRT* model is limited by the first deformable mode of the belts that lies approximately at frequency of 60–80 Hz.

The equations of motion that govern the tyre structural model are:

$$[M_s]\ddot{\mathbf{q}}_s + [C_s]\dot{\mathbf{q}}_s + [K_s]\mathbf{q}_s = \mathbf{F}_p(\mathbf{q}_{be}, \dot{\mathbf{q}}_{be}, \mathbf{q}_s, \dot{\mathbf{q}}_s) + \mathbf{F}_{nl}(\mathbf{q}_s, \dot{\mathbf{q}}_s) + \mathbf{F}_h, \tag{1}$$

where $\mathbf{q}_s$ and $\mathbf{q}_{be}$ are, respectively, the vectors of the structure's and of the brush elements' degrees of freedom, $[M_s]$, $[C_s]$ and $[K_s]$ are the mass, damping and stiffness

matrices of the tyre structure and $\mathbf{F}_p$, $\mathbf{F}_{nl}$ and $\mathbf{F}_h$ are the vectors of the forces between tyre structure and tyre contact, of the non-linear effects (such as gyroscopic effects) and of the generalized external forces applied to the hub.

2.2. The Tyre Contact Model

In order to correctly estimate tyre wear, the real local contacting conditions have to be determined both in terms of contact forces and slip velocities. Thus, the tyre contact model has to take into account the real geometry of the tyre tread design and the tread material dynamic behaviour.

The adopted tyre contact model can be classified as a 2D brush model (Figure 1b, [3,4]): each brush element has two degrees of freedom, the longitudinal and lateral displacements in the contact plane. The tyre rolling surface is gridded using a rectangular grid with uniformly spaced knots in circumferential direction and a non-uniformly spaced knots in axial direction. Each grid element corresponds to a brush element. Thus, mass, damping and stiffness of each brush is a function of its position on the tyre rolling surface. While the mass is a function of the aspect ratio of each grid element, the damping and stiffness characteristics of the brushes (between adjacent brushes and between the given brush and the belts) are a function of the rubber temperature, of the excitation frequency, of the pre-strain, etc. (viscoelastic behaviour of rubber). In order to simplify the tyre dynamic simulations, these stiffness and damping parameters are determined at a working temperature of 70 °C and at an excitation frequency of 100 Hz (mean excitation frequency of the tread elements due to road texture at the various vehicle speeds) through a linearized FEA model of the tyre tread design for different imposed vertical loads.

At present, the normal contact problem, i.e., the determination of the contact area shape and of the contact pressure distribution, has to be solved externally either using experimental tests or FEA simulations taking into account the influence of the vertical load applied at the hub, of the camber angle and of the yaw angle.

The equations of motion of the tyre contact model are

$$[M_{be}]\ddot{\mathbf{q}}_{be} + [C_{be}]\dot{\mathbf{q}}_{be} + [K_{be}]\mathbf{q}_{be} = \mathbf{F}_p(\mathbf{q}_{be}, \dot{\mathbf{q}}_{be}, \mathbf{q}_s, \dot{\mathbf{q}}_s) + \mathbf{F}_c(\mathbf{q}_{be}, \dot{\mathbf{q}}_{be}), \tag{2}$$

$[M_{be}]$, $[C_{be}]$ and $[K_{be}]$ being the mass, damping and stiffness matrices of the tyre contact and $\mathbf{F}_c$ the vector of the frictional contact forces.

The contact friction force vector of the ijth element (i being the index of the generic element along the circumferential direction and j being the index of the generic element along the transversal direction) is equal to:

$$\begin{array}{ll} \mathbf{F}_{c_{ij}} = \left[C_{be_{ij}}\right]\Delta\dot{\mathbf{q}}_{be_{ij}} + \left[K_{be_{ij}}\right]\Delta\mathbf{q}_{be_{ij}} & \left|\mathbf{F}_{c_{ij}}\right| \le \mu_{s_{ij}} F_{n_{ij}}, \\ \mathbf{F}_{c_{ij}} = -\mu_{d_{ij}} \cdot F_{n_{ij}} \cdot \dfrac{\mathbf{v}_{ij}}{|\mathbf{v}_{ij}|} & \left|\mathbf{F}_{c_{ij}}\right| > \mu_{s_{ij}} F_{n_{ij}} \end{array} \tag{3}$$

in which the two working conditions, sticking (adhesion) and sliding, have been separated. In this equation $\mathbf{F}_{c_{ij}}$ is the vector of the frictional contact forces on the ijth brush, $\left[C_{be_{ij}}\right]$ and $\left[K_{be_{ij}}\right]$ are, respectively, the damping and stiffness matrices of the ijth brush, $\Delta\mathbf{q}_{be_{ij}}$ is the vector of the deformation of all elastic elements linked to the ijth brush, $\mu_{s_{ij}}$ and $\mu_{d_{ij}}$ are the static and dynamic friction coefficients, $F_{n_{ij}}$ is the normal contact force (equal to $p_{ij}\Delta x_{ij}\Delta y_{ij}$, p_{ij} being the contact pressure on the

ijth brush, Δx_{ij} and Δy_{ij} the longitudinal and lateral dimensions of the ijth brush respectively) and $\mathbf{v}_{ij}$ is the sliding speed vector of the ijth brush.

2.3. The complete PaRRT Model

The equations of the complete tyre model are integrated in the time domain using a variable order multistep Adams – Bashforth – Moulton PECE solver. At any time instant during the simulation, stiffness and damping matrices of the structural tyre model (equation (1)) are re-computed as function of the actual vertical load while the stiffness and damping matrices of the contact tyre model (equation (2)) are determined as function of the local pressure value (different from brush to brush).

3. The Local Friction Model

In order to integrate the friction law into the tyre model, a simpler approach than experimental data tables to be interpolated at any integration step and for any brush element would be desirable. One simple and well-accepted empirical formulation for the friction of rubber compounds that takes into account various external parameters is Savkoor's friction law [5]:

$$\mu_{\mathrm{d}_{ij}} = \left(\frac{p_{ij}}{p_0}\right)^{-k} \left[\mu_0 + (\mu_{\mathrm{m}} - \mu_0) \exp\left\{-h^2 \log^2\left(\frac{|\mathbf{v}_{ij}|}{v_{\mathrm{m}}}\right)\right\}\right]. \tag{4}$$

p_0 being the reference contact pressure, k the pressure exponential factor, μ_0 and μ_{m} the starting friction coefficient (assumed to be equal to the static friction coefficient $\mu_{\mathrm{s}_{ij}}$) and the maximum value of the friction coefficient, v_{m} the sliding speed at which the maximum value of the friction coefficient is achieved and h the speed parameter.

The friction law parameters are a function of the rubber compound, not of the ijth element considered. As such, Savkoor's friction law considers the dependency of friction only from sliding speed and normal pressure. However, the same empirical formula can be used introducing the dependency of surface roughness and rubber/surface temperature just assuming that the above parameters are not constant but are a function of these two quantities. The relationship between Savkoor's friction law parameters and surface roughness/temperature has to be determined experimentally and therefore the experimental data collected from the designed tribometer are necessary.

In fact, in order to simplify the friction model and due to the fact that tyre tread characteristics are linearized at a given fixed temperature, also Savkoor's friction law parameters have been identified at that temperature (70 °C for car tyres). Moreover, knowing the track on which the tyre will have to drive, the mean micro-texture of the asphalt is determined. Savkoor's friction law parameters are then identified on an abrasive surface having the same mean micro-texture. Hence, during tyre dynamic simulations all Savkoor's friction law parameters are assumed to be constant. Figure 2 shows the identified friction law curves for five values of normal pressure for the two considered compounds.

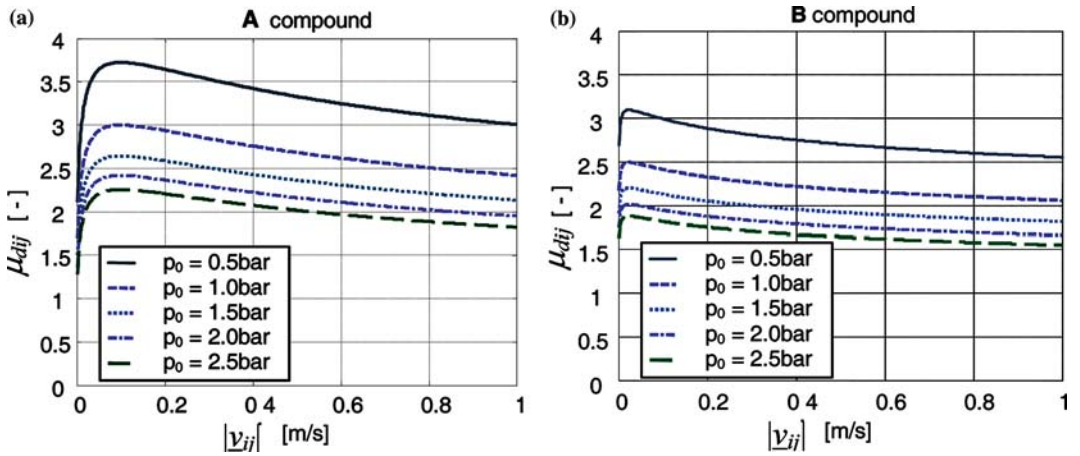

Figure 2. Local friction law curve of the two tread compounds considered at 70 °C rubber bulk temperature and a surface micro-texture having mean wavelength equal to 2.3×10^{-4}m.

4. The Local Wear Model

Rubber wear is the result of several different mechanisms that range from rubber oxidation to mechanical delamination. All or part of these mechanisms may be present at the same time thus making it very difficult to build up a predictive and at the same time practical model for rubber wear. Moreover, rubber wear is a function of a huge variety of external parameters such as the shape of the contacting surfaces, the presence of contaminants between these surfaces, the sliding speed, the normal pressure, the contact temperature, etc. [6]. Thus, it is very important to test the specimen in conditions similar to those of real working conditions. This observation could imply that outdoor tests on real tyres are the preferred way to collect wear data. Outdoor tests however, besides being very expensive, add enormous complexity to the understanding of the wear phenomenon. Hence, starting from experimental tests carried out under laboratory conditions, a heuristic local wear law applicable in all different working conditions of the tyre is searched for.

To test the validity of local wear law concept, experimental wear tests were carried out on two different testing machines, an imposed slip angle testing machine and an imposed rotational slippage testing machine. Since the two rubber specimens for the two testing machines have completely different geometry, in order to be able to compare the wear results it is necessary to normalize both the frictional power (i.e., the power dissipated at the contact due to friction) and the mass loss: the frictional power is scaled with the contact area while the mass loss is divided by the travelled distance times the specimen's transversal dimension (covered area). The obtained wear results fall on the same curve (Figure 3). This means that, although the wearing conditions of the two machines are completely different (imposed slip angle and imposed slippage), this representation correctly describes the abrasion process, i.e., the local wear law.

In order to be implemented into the tyre dynamical model, the local wear results have to be summed up into some compact analytical formula. The frictional power per unit contact area vs. mass loss per unit covered area relation may be

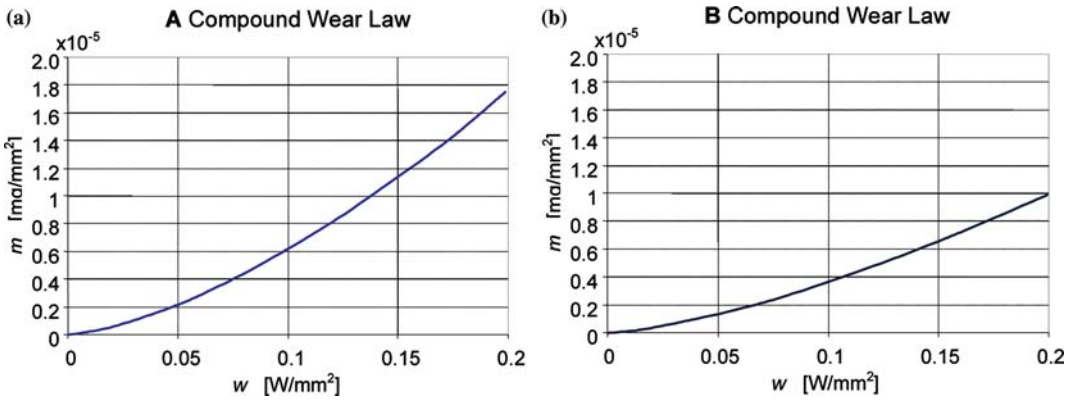

Figure 3. Local wear law curve of the two tread compounds considered at 70 °C rubber bulk temperature and a surface micro-texture having mean wavelength equal to 2.3×10^{-4}m.

approximated by the following expression:

$$\tilde{m}_{ij} = k_1 \tilde{w}_{ij}^{k_2}, \tag{5}$$

where $\tilde{m}_{ij}$ is the mass loss per unit covered area, $\tilde{w}_{ij}$ is the frictional power per unit contact area and k_1 and k_2 are the wear constants of the rubber compound function of temperature and surface roughness.

The identified local wear laws for the two tyre tread compounds at 70 °C and on an abrasive surface with mean micro-texture equal to the one measured on the real track are shown in Figure 3. During the simulation with *PaRRT* model, once the tangential traction distribution and the slip velocity distribution inside the contact area have been determined at each integration step, the local wear law is applied to each brush element and the obtained wear distribution is stored. Under the hypothesis of a linear wear process, the wear distributions may be superimposed thus obtaining the worn 3D tyre profile.

5. Experimental – Numerical Comparison

In order to validate the wear prediction tyre model, full-scale outdoor experimental tests were carried out. The wear tests were performed using two Peugeot 406 HDi passenger cars driving in a convoy along a 129 km long track. Both Peugeot 406's are tested in fully loaded conditions (using water dummies on all available empty seats). The test track, representing typical European roads and traffic situations, is the CISA road course in Italy. This track was repeated several times to achieve a total travelled distance of 8000 km. The tests were repeated twice, in summer and in winter, in order to determine the influence of external weather conditions on tyre wear. The results shown below are referred to the summer test campaign. To numerically simulate the wear results of the winter test campaign, the local friction as well as the local wear laws should be changed.

Since no hub forces were acquired, to compare experimental and numerical wear data an intermediate step is necessary: using a validated vehicle's multi-body model

that reproduces the (acquired) working conditions of the vehicle, the time histories of the hub forces can be numerically reconstructed.

In order to numerically reproduce the tyre tread wear measured on the CISA road course, a selection of the manoeuvres performed has to be carried out in order to reduce simulation time. However, the number of manoeuvres should not be too small in order to reproduce the real track. Thus, a pre-analysis of all the different manoeuvres performed on the CISA road course has been carried out in order to classify the acquired manoeuvres from a wear point of view. This pre-analysis is based on a single track vehicle model. The load transfer from left to right wheel (and viceversa) due to curve negotiation is determined statically, i.e., no roll motion of the carbody is allowed. The 36 most wearing manoeuvres are selected thus obtaining a "virtual" travel profile on which the tyre wear behaviour has to be analyzed. These manoeuvres are then simulated using an MB vehicle model (ADVANCE, [7]) of the Peugeot 406 HDi vehicle in order to determine the time histories of the generalized hub forces at the four tyres. These forces, together with the slip angle and the camber angle at the hub, are fed into *PaRRT* model to determine the wear distribution on the tyre rolling surface.

5.1. Numerical Evaluation of the Wear Distribution

To determine the mass loss distribution $\tilde{M}_{ij}$ over the tyre rolling surface, the local mass loss distributions are re-positioned on the tyre rolling surface and summed up (k being the counter on all the time instants at which the ij^{th} brush element is in contact):

$$\tilde{M}_{ij} = \sum_{k} \tilde{m}_{ij}(k) \cdot \Delta y_{ij} \cdot v_{x_{ij}}(k) \cdot \mathrm{d}t, \tag{6}$$

where $\tilde{M}_{ij}$ is the mass loss distribution, $v_{x_{ij}}$ is the longitudinal component of the sliding speed of the ijth brush and dt is the integration step.

The transversal tyre wear profile is obtained by summing along the circumferential direction. The mean wear, instead, can be determined by summing along both the circumferential and axial directions.

5.2. Comparison Between Numerical and Experimental Total Wear Depth Rate

As previously described, the selected manoeuvres are significantly less than the real manoeuvres performed on the CISA road course. To be able to compare the simulated wear results to the experimentally measured ones, an extrapolation procedure based on the mean wear (normalised with respect to the length of the manoeuvre) has been set up. Since the mean wear is a function of the longitudinal and lateral acceleration of the car and of the vehicle speed, a 4D hyper-surface interpolating the simulated wear data can be identified. Then, through Delaunay triangulation method ([8]), the mean wear (in steady-state conditions) of any manoeuvre performed on the CISA road course can be calculated (a linear extrapolation method for out of range values is used). Note that the hyper-surface does not account for evolving changes in the tyre characteristics due to tread loss. Thus, the order of the simulations is not

important. This assumption implies that, although the local wear law is non-linear, the global tyre wear law seems to be fairly linear with the mileage (at least for a short track length).

As a result of the linearity assumption made, the calculated mean wear values can be summed up in order to determine the total wear amount M (in kg) over the whole CISA road course. In order to be able to compare the simulated results with the experimental wear data, a conversion from the total wear amount to the total wear depth rate (in mm/km) is necessary:

$$\Delta h = \frac{(M/L_{\mathrm{CISA}})}{\rho \cdot 2\pi R \cdot d}. \tag{7}$$

Δh being the total wear depth rate, M the total wear amount, L_{CISA} the total length of the CISA road course before each wear measurement, ρ the density of the tread rubber compound, R the tyre nominal radius and d is the tyre width.

Due to the fact that tyre characteristics as well as tyre geometry change with the mileage (i.e., with the tyre wear) at least the tyre contact model (together with the pressure distributions) should be updated after a certain number of manoeuvres. However, during the present research no update was carried out. Thus, the estimated wear diverges from the measured one as the mileage increases. It was therefore decided to compare the simulated tyre wear with the experimental one after 4000 km (first wear measurement).

Figure 4 shows the comparison between the experimental total wear depth rate Δh and the measured one. The values have been normalized with respect to the maximum wear depth rate that, for both tyre sets, is the one of the right front tyre (due to the asymmetry of the CISA road course). Both tyre sets show that the two front tyres (LF, RF) wear more than the two rear tyres (LR, RR). This is due to the fact that the front tyres are steered and the centre of gravity of the Peugeot 406 HDi cars is slightly in front of the geometric centre of the car. The tyre model correctly reproduces the scaling between the four tyres of the same type. Also the quantitative differences between the normalized total wear depth rate are quite correctly estimated (in the worst case an underestimation of less than 35% occurs).

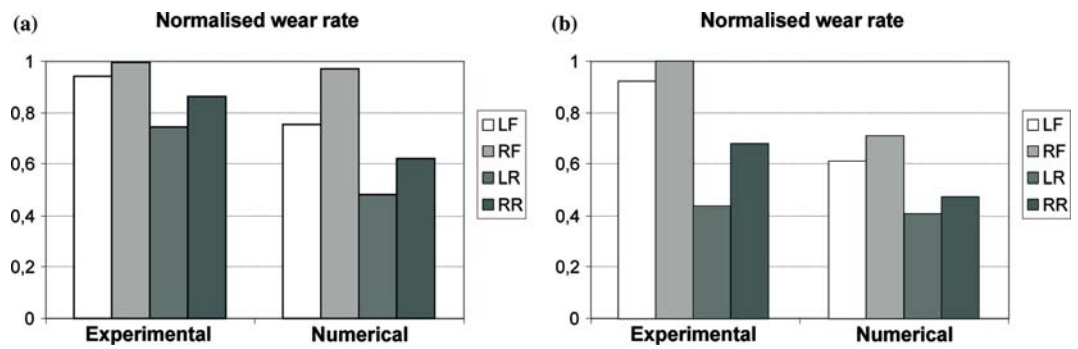

Figure 4. Comparison between the experimental and numerical total wear depth rate normalized with respect to the maximum wear depth rate for A tyres (a) and B Tyres (b) after 4000 km.

6. Sensitivity Analysis of the Model's Parameters With respect to Wear

6.1. Wear Computation Procedure

The process of tyre wear evaluation can be split into the following steps:

1. by modifying one per time the structural parameters and tread compound characteristics of A tyre, new "virtual" tyres were generated; note that it is assumed that each tyre physical parameter can be changed independently from the others; this is obviously not true but indications on how to reduce wear can nevertheless be obtained;
2. since *PaRRT* model is very heavy from a computational point of view, it is necessary to find a way around for vehicle dynamic simulations; using the model in "testrig" mode a pre-analysis has been carried out to fully characterise each virtual tyre in both pure and combined slip conditions (steady state and transient);
3. a 14 d.o.f. mathematical model of a segment C car, implementing a table lookup procedure to describe the tyre-road interaction, is "driven" along a test track (made up of a sequence of manoeuvres reproducing the most typical working conditions of a tyre) by a simple driver model with speed targets; the time histories of the generalised hub-forces are thus determined;
4. the sequence of manoeuvres of the ideal track is reproduced by *PaRRT* model operated in "simulation" mode, and the wear of each virtual tyre is stored.

Virtual tyres are generated by changing, one per time, of ±25% the 20 tyre model's parameters shown in Table 1.

Note that friction law and wear law parameters are kept constant even when tread compound stiffness and damping values are modified. Figures 5 and 6 show the friction circle diagrams $F_y - F_x$ and $M_z - F_x$ for one of the virtual tyres considered at different vertical loads: 3000 N (a), 4500 N (b) and 6000 N (c).

The ideal track should satisfy two opposite requirements: it should contain as many manoeuvres as possible but it should be as short as possible (for computational reasons). The best compromise is shown in Figure 7.

A detailed description of the track is given in Table 2 together with the speed profile imposed for each of the 11 sections. The last two columns of Table 2 show the maximum longitudinal and lateral accelerations that can be achieved in each section. It can be seen that also very aggressive manoeuvres are considered (combined braking/accelerating and cornering manoeuvres with high longitudinal and lateral accelerations). The double lane change manoeuvre of Section 6 consists on a lateral shift of 5 m and aims at reproducing an overtaking condition on a highway. The track has a total length of 1500 m covered in about 55 s with a mean speed of 100 km/h.

A 14 d.o.f. vehicle model was developed in Matlab/Simulink environment: the chassis is treated as a rigid body (six dofs) and each wheel has two degrees of freedom, the vertical travel and the rotation about its axis. Suspensions are introduced by means of a quasi-static characterisation and a tyre lookup table model is used to describe tyre–road interaction. Also the driveline, the braking system and the powertrain are modelled. The vehicle model is combined with a very simple driver model

Table 1. List of the tyre structural parameters and of tread compound properties

Symbol	Description
K_{sy}	Hub-Belt lateral stiffness
K_{sx}	Hub-Belt longitudinal stiffness
K_{sc}	Hub-Belt camber stiffness
K_{st}	Hub-Belt torsion stiffness
K_{rz}	Vertical reidual stiffness
K_{rx}	Lateral residual stiffness
K_{rc}	Camber residual stiffness
K_{rt}	Yaw residual stiffness
R_{sy}	Hub-Belt lateral damping
R_{sx}	Hub-Belt longitudinal damping
R_{sc}	Hub-Belt camber damping
R_{st}	Hub-Belt torsion damping
R_{rz}	Vertical residual damping
R_{rx}	Lateral residual damping
R_{rc}	Camber residual damping
R_{rt}	Yaw residual damping
EJ	Equivalent beam
ρ	Tread compound density
E'	Tread compound stiffness
$\tan\delta$	Tread compound damping

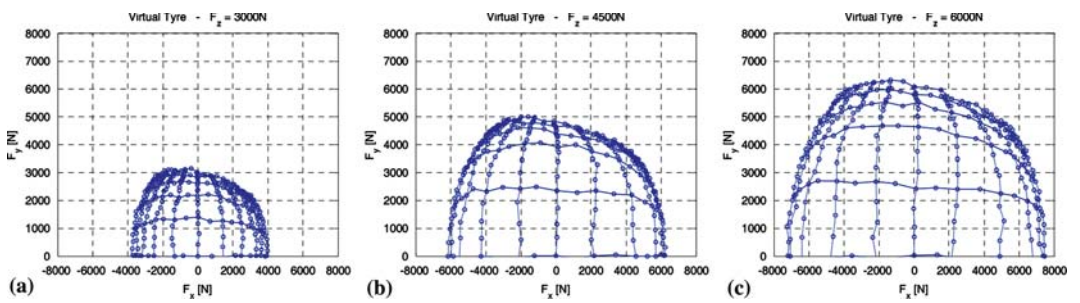

Figure 5. Friction circle diagram $F_y - F_x$ of a virtual tyre at different vertical loads: 3000 N (a), 4500 N (b) and 6000 N (c).

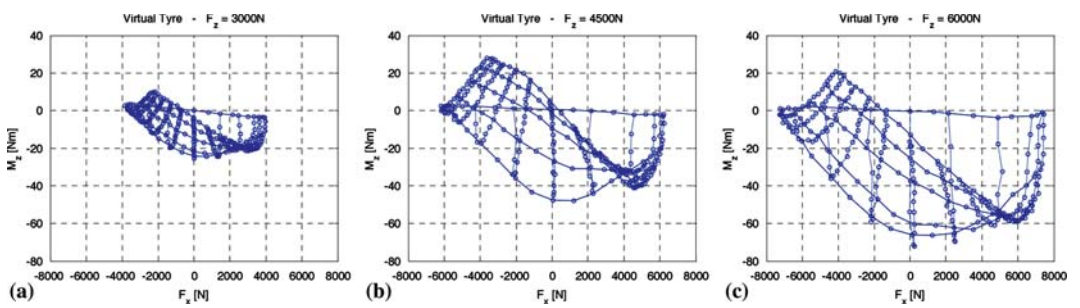

Figure 6. Friction circle diagram $M_z - F_x$ of a virtual tyre at different vertical loads: 3000 N (a), 4500 N (b) and 6000 N (c).

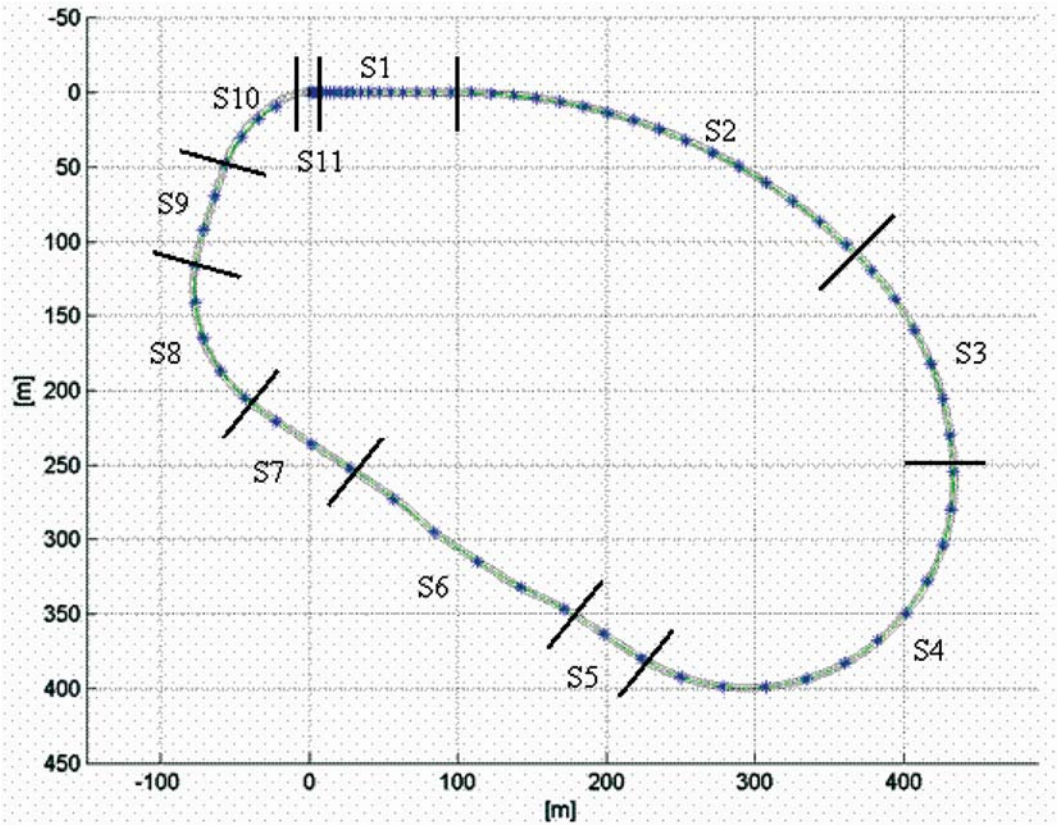

Figure 7. Top view of the virtual track.

Table 2. Description of the virtual track sections

Section	Description	Length (m)	Initial speed (km/h)	Final speed (km/h)	Radius (m)	Longitudinal acceleration (m/s^2)	Lateral acceleration (m/s^2)
S1	Straight track	100	0	50	∞	0.96	0.0
S2	Curve	300	50	90	385	0.72	0.5–1.6
S3	Curve	166	90	90	208	0.00	3.0
S4	Curve	300	90	110	139	0.51	4.5–6.7
S5	Straight track	50	110	130	∞	3.70	0.0
S6	Double lane change	150	130	130		0.00	
S7	Straight track	100	130	90	∞	−3.40	0.0
S8	Curve	130	90	90	100	0.00	6.2
S9	Straight track	90	90	80	∞	−0.73	0.0
S10	Curve	80	80	40	80	−2.31	6.2–1.5
S11	Straight track	20	40	0	∞	−3.09	0.0

that follows the assigned trajectory (steer angle control) and the speed profile (accelerator/brake control).

The time histories of the generalised hub forces on the four tyres are outputted by the vehicle's dynamic simulations. These time histories are fed into *PaRRT* model in "simulation" mode to determine tyre wear. In fact, only the front (driven) tyres are considered due to their higher wear amount. Thus the following results are related to the front (driven) tyres.

6.2. Sensitivity Analysis

Table 3 shows the difference (in percentage) between the virtual tyres obtained by changing one of the structural parameters of the reference tyre from a wear point of view (total wear amount). Column 3 reports the difference for −25% variations while column 4 shows the difference for +25% variations.

As can be noticed only the hub-belt lateral stiffness, the hub-belt longitudinal stiffness and hub-belt torsion stiffness seem to have a small influence on tyre wear. A decrease of the hub-belt lateral stiffness leads to an increase of the wear amount of about 7%; an equal increase of the same parameter only leads to a decrease of amount of 1.5%, thus indicating the presence of a non-linear effect. The role of the hub-belt lateral stiffness is probably related to the cornering stiffness of the tyre: if the lateral stiffness is decreased, the same lateral force can be developed with an higher slip angle, thus giving rise to an increase in frictional power and finally in wear. A decrease of the residual stiffness does not cause the same variation due to

Table 3. Effect of structural parameter change on tyre wear

Symbol	Description	−25%	+25%
K_{sy}	Hub-belt lateral stiffness	+6.9%	−1.4%
K_{sx}	Hub-belt longitudinal stiffness	−3.9%	+2.1%
K_{sc}	Hub-belt camber stiffness	+0.9%	−1.2%
K_{st}	Hub-belt torsion stiffness	−4.9%	+0.2%
K_{rz}	Vertical reidual stiffness	−0.9%	+0.9%
K_{rx}	Lateral residual stiffness	+0.5%	n.a.
K_{rc}	Camber residual stiffness	−0.7%	+0.4%
K_{rt}	Yaw residual stiffness	+0.7%	−0.1%
R_{sy}	Hub-belt lateral damping	−1.0%	+0.1%
R_{sx}	Hub-belt longitudinal damping	+0.2%	−0.9%
R_{sc}	Hub-belt camber damping	−0.5%	+0.1%
R_{st}	Hub-belt torsion damping	−1.9%	+0.1%
R_{rz}	Vertical residual damping	−1.7%	+0.9%
R_{rx}	Lateral residual damping	+0.4%	−2.1%
R_{rc}	Camber residual damping	−1.4%	+0.7%
R_{rt}	Yaw residual damping	+1.3%	−1.5%
EJ	Equivalent beam	+0.8%	−1.6%

Table 4. Effect of tread compound parameter change on tyre wear

Symbol	Description	−25%	+25%
ρ	Tread compound density	+32.5%	−23.3%
E'	Tread compound stiffness	+55.5%	−31.9%
$\tan\delta$	Tread compound damping	+18.0%	−16.0%

the fact that residual and hub-belt stiffness are connected in series and residual quantities are an order of magnitude higher than hub-belt ones.

The effects of the hub-belt torsional stiffness and of the hub-belt longitudinal stiffness are similar: a decrease of any of these parameters leads to a reduction of the longitudinal tyre stiffness of the tyre. This means that the same longitudinal force can be achieved with higher longitudinal slip. This property seems to affect the tyre behaviour mainly in combined slip conditions (i.e., accelerating while cornering).

Table 4 shows the differences (in percentage) between the virtual tyres obtained by changing one of the tread characteristics of the reference tyre from a wear point of view (total wear amount).

The properties of the tread compound deeply affect tyre wear. An increase in the tread compound density determines a higher inertia of the brushes, thus leading to lower slip velocities, lower frictional power and lower wear. An increase in the tread compound stiffness leads to a stiffer tyre (the same longitudinal/lateral force can be obtained with lower slip - pages/slip angles) thus to lower frictional power and lower wear.

An increase in $\tan\delta$, and thus of the damping factor of the tread compound, leads to smaller slip velocities once adhesion thus leading to a reduced frictional power and wear.

7. Conclusions

The proposed tyre dynamical model allows to predict the tyre wear both qualitatively (see the correct scaling of the eight considered tyres) and quantitatively (the highest relative error is equal to less than 35% and is referred to the left rear A tyre) over a given track once the tyre structural and contact parameters, as well as the local friction and wear laws, are known. The validation of the model was carried out in terms of total wear depth rate. Great attention has to be paid to the tyre contact grid. Otherwise, the tyre wear will probably be underestimated as is the case of B tyre. Moreover, in order to correctly determine tyre wear over a long track, several iterations of vehicle model and tyre model simulations are necessary.

Moreover, a numerical procedure to investigate the effect of tyre design parameters on tyre wear was setup. A series of "virtual" tyres was generated by varying each single parameter of the physical tyre model by ±25%. The virtual tyres wear behaviour was compared with the wear behaviour of a reference tyre on an ideal track using a segment C car model driven by a very simple driver model. As expected, the sensitivity analysis showed that the tread compound properties are the ones that mostly

affect the slip distribution inside the contact footprint and thus the wear behaviour of the tyre. An increase in tread compound density, stiffness and damping would lead to a sensible reduction of tyre wear (respectively, around 20%, 30%, 15%). It should however by taken into account that these improvements are achievable only by keeping friction and wear properties of the tyre constant.

Although the "best tyre" obtained from this work may not be obtainable with the present technological solutions, this analysis provides a quantitative indication of which of the tyre parameter is most effective to reduce tyre wear.

We greatly acknowledge the European Community for having founded this research and all the other partners of the *TROWS* project, especially TNO, the project co-ordinator, Pirelli and Nokian Tyres, who carried out the tests for the determination of the local wear law, and Helsinki University of Technology, who instrumented the vehicles for the outdoor tests.

References

1. Mancosu, F., Sangalli, R., Cheli F. and Braghin, F., ' Mathematical-physical 3D tire model for handling/comfort optimization on a vehicle: Comparison with experimental results', *Tire Sci. Technol.* **28** (4) (2000) 210–232.
2. Braghin, F., Cheli, F., Scaltritti, D. and Tomasini, G., 'Rigid-Ring Tyre Model: Out-of-Plane Parameter Identification from Experimental Tests on Rolling Tyre', in: *Proceedings of the 8th VSDIA Conference on Vehicle System Dynamics Identification and Anomalies*, Budapest, Hungary, 2002.
3. Lacombe, J., *Tire Model for Simulations of Vehicle Motion on High and Low Friction Road Surfaces*, Winter Simulation Conference Proceedings, Orlando, Florida, USA, 2000.
4. Pacejka, H.B., *Tyre and Vehicle Dynamics*, Butterworth-Heinemann, The Netherlands, 2002, p. 612
5. Persson, B.N.J., 'Theory of Rubber Friction and Contact Mechanics', *J. Chem. Phys.* **115** 8 (2001) 3840–3861.
6. Han, S.C. and Han, M.H., 'Fracture Behavior of NR and SBR Vulcanizates Filled With Ground Rubber Having Uniform Particle Size', *J. Appl. Polymer Sci.* **85** 12 (2002) 2491–2500.
7. Van den Tillaart, E., Mourat, S. and Lupker, H.A., ' TNO-ADVANCE, A Modular Simulation Tool for Combined Chassis and Powertrain Analysis', in: *Proceedings of the AECV Conference*, Noordwijk, The Netherlands, 2002.
8. Chrisochoides, N. and Demian, N., 'Parallel Delaunay Mesh Generation Kernel', *Int. J. Numer. Methods Eng*, **58** (2) (2003) 161–176.